

Ammar M. Abdilghanie · Peter J. Diamessis

On the generation and evolution of numerically simulated large-amplitude internal gravity wave packets

Received: 15 February 2010 / Accepted: 15 October 2010
© Springer-Verlag 2011

Abstract Numerical simulations of internal gravity wave (IGW) dynamics typically rely on wave velocity and density fields which are either generated through forcing terms in the governing equations or are explicitly introduced as initial conditions. Both approaches are based on the associated solution to the inviscid linear internal wave equations and, thus, assume weak-amplitude, space-filling waves. Using spectral multidomain-based numerical simulations of the two-dimensional Navier–Stokes equations and focusing on the forcing-driven approach, this study examines the generation and subsequent evolution of large-amplitude IGW packets which are strongly localized in the vertical in a linearly stratified fluid. When the vertical envelope of the forcing terms varies relatively rapid when compared to the vertical wavelength, the associated large vertical gradients in the Reynolds stress field drive a nonpropagating negative horizontal mean flow component in the source region. The highly nonlinear interaction of this mean current with the propagating IGW packet leads to amplification of the wave, a significant distortion of its rear flank, and a substantial decay of its amplitude. Scaling arguments show that the mean flow is enhanced with a stronger degree of localization of the forcing, larger degree of hydrostaticity, and increasing wave packet steepness. Horizontal localization results in a pronounced reduction in mean flow strength mainly on account of the reduced vertical gradient of the wave Reynolds stress. Finally, two techniques are proposed toward the efficient containment of the mean flow at minimal computational cost. The findings of this study are of particular value in overcoming challenges in the design of robust computational process studies of IGW packet (or continuously forced wave train) interactions with a sloping boundary, critical layer, or caustic, where large wave amplitudes are required for any instabilities to develop. In addition, the detailed description of the dynamics of the wave generation region may offer a first probe into the underlying physics of disruptive near-source nonlinearities observed in laboratory experiments of persistently forced IGW beams. Finally, the question arises as to whether a highly vertically compact IGW packet, which has propagated far from its source but still maintains its original structure and amplitude, can indeed occur in nature.

Keywords Stratified flows · Internal gravity wave packets · Wave generation and propagation · Wave-driven mean flow

Communicated by: Klein

A.M. Abdilghanie
Department of Mechanical Engineering, University of Washington, Seattle, WA 98195, USA
E-mail: aelghany@uw.edu

P. J. Diamessis (✉)
School of Civil and Environmental Engineering, Cornell University, Ithaca, NY 14853, USA
E-mail: pjd38@cornell.edu

1 Introduction

1.1 Remote interactions of internal gravity wave packets

Internal gravity waves (IGWs) are ubiquitous in the stratified interior of the ocean, lakes, and atmosphere [6]. They are capable of transporting energy over very long distances before depositing it far from the wave generation site through localized breaking events in mid-water/air or near boundaries [30]. In the study of IGW breaking, it is commonly assumed that the IGW under consideration is space filling and of persistent duration. However, because of the transience in their generation, previously encountered nonlinear interactions in mid-water/air and the finite dimension of their source, IGWs often propagate as relatively short packets or groups of finite extent in one or more spatial dimensions. This limited extent can bear significant implications in characterizing the transmission, reflection, and dissipation of an IGW interacting with a critical layer, sloping boundary, or caustic [29]. Important insight into the highly nonlinear physics of such interactions has been obtained through numerical process studies based on Direct Numerical or Large Eddy Simulations (DNS or LES) [5, 14, 15, 22, 31].

Transmission/reflection phenomena and the additional turbulence/mixing due to breaking that accompany the interaction of an IGW with current shear, sloping topography, or variable background stratification are sensitive to large wave amplitude, particularly wave steepness which is defined as the ratio of the isopycnal displacement amplitude, A_ζ , to the horizontal wavelength, λ_x . The sensitivity of IGW dynamics is strongest the closer the initial wave steepness is to the corresponding limit value for breaking [25]. Therefore, it is imperative that a DNS/LES study of IGW propagation and breaking be equipped with a wave generation mechanism that minimizes transients and allows maximum flexibility in choice of wave steepness without altering the externally prescribed wave structure, vertical extent, and characteristic properties (amplitude, primary frequency/wavelength and group/phase velocity predicted by linear theory). In particular, when a vertically localized IGW packet is required, it must remain robust both near the source but also during its subsequent propagation away from the source, prior to its arrival at the interaction region.

1.2 Generation of numerically simulated internal gravity waves

Two approaches are used to produce the initial IGW field in numerical process studies: One strategy designates an initial condition as a prescribed perturbation of the density and velocity fields or velocity stream functions in the form of an exact solution of the linearized internal wave equations [18, 27, 31]. An alternative approach consists of introducing into the governing equations appropriately specified mechanical forcing (body force) terms, operative within a prescribed generation region [5, 9, 22]. The forcing can either have finite duration [11] or persist throughout the entire simulation [9, 22, 32] generating either a localized packet or a continuous wave train, respectively. The mechanical forcing approach is preferred as it allows greater control over the time scale of energy injection into the IGW field and enables a closer comparison with laboratory experiments, as the structure of the forcing terms can be modeled after that of experimental IGW generators (such as the one described in reference [12]). Furthermore, the mechanical forcing has the advantage of allowing the initial IGW to develop more “naturally”, i.e., within the constraints of the Navier–Stokes equation, which is particularly suitable for higher-order accuracy element-based flow solvers, such as the one used in the present study [7]. High-order accuracy numerical codes can be particularly sensitive to initial/boundary conditions and forcing that are not exact solutions of the governing equations [3], as persistent and disruptive transients develop [8].

1.3 Nonlinearity and dispersion in internal gravity wave generation and propagation

The requirement of a wave packet with a finite spatial extent poses its own set of numerical challenges in terms of sustaining a packet structure that is robust and well defined both as the packet leaves the source region and also as it propagates toward a remote interaction region. The efficient design of mechanical wave forcing has been examined by Slinn and Riley [22]. By analyzing the *linearized* equations of motion augmented with forcing, they found that for the envelope of the emerging signal to be steady and uniform in shape, the vertical extent of the forcing region has to be larger than one vertical wavelength. When the forcing region is narrower than a vertical wavelength, the emitted signal is modulated by an irregular, non-constant envelope. Additional challenges for maintaining a robust spatial structure are brought about when large wave amplitudes are required, on account of the enhanced wave dispersion when compared to that of a weak-amplitude wave [31].

As we will illustrate, by means of mean flow generation, nonlinear effects can also produce significant distortion and weakening of a large-amplitude wave packet that is strongly localized in the vertical. Such effects are highly undesirable when large wave amplitude is a necessary condition for IGW breaking to occur in any of the interaction scenarios described above. The formation of residual mean flows in the generation region of numerically simulated IGWs has been observed (although not reported) by Slinn and Riley who focused on the study of the reflection of IGWs off a sloping boundary and used a rotating coordinate system and forcing terms identical to those considered here [22,23]. A Rayleigh damping/sponge layer aligned with the top boundary of the domain enabled the absorption of the residual mean flow (D. N. Slinn, personal communication). Although sponge layers can potentially remove the mean flow, they are computationally expensive as they tend to be rather thick and consume a large number of grid points (e.g., $O(10\%)$ of the grid points in the slope-normal direction in the above study [22]).

Issues of mean flow generation were later reported by Zikanov and Slinn [32] for a similar flow configuration where an obliquely incident IGW was considered. During the initial transient adjustment phase of the simulations, before the wave reached the bottom slope, a mean flow was observed in the along-slope direction at the propagating front of the wave and explained on the basis of the local transient change in Reynolds stress in front of the wave. Another along-slope mean flow, nonpropagating in nature, was also generated in the forcing region in a direction opposite to that produced at the wave front and was attributed to the Reynolds stress gradient in the slope-normal direction which is caused by the growth of the wave as it passes through the forcing region.

1.4 Objectives

So far, no systematic study has been published, which is aimed toward understanding the underlying cause of residual mean flow formation associated with the generation of large-amplitude IGW packet that is strongly localized in the vertical, its impact on the long-time evolution of the wave field, and the identification of possible mean flow containment mechanisms. Most previous numerical studies have focused on the interactions between wave and wave-induced mean flow for quasi-plane moderate to large-amplitude IGW packets introduced as initial conditions [25,27,28]. Thus, our fundamental working hypothesis is that additional nonlinear effects may emerge when combining strong vertical localization, large wave amplitude, and possibly finite duration forcing. All of the above factors may force strong adjustment of the solution of the fully nonlinear governing equations away from their externally prescribed linear counterpart and, as a result, may nontrivially alter the subsequent evolution of the wave field.

We first examine the near-source distortion of a forcing-generated vertically localized IGW packet as a function of stratification strength and degree of horizontal localization. Motivated by the insight originally offered by Zikanov and Slinn [32], we then use scaling arguments to identify the dependence of the magnitude of the associated mean flow on wave steepness, degree of vertical localization, and degree of wave hydrostaticity. The understanding gained enables the design of efficient mean flow containment techniques that allow the mechanical forcing-driven numerical generation of a well-defined IGW packet robustly propagating toward a nearby interaction region. Since mechanical forcing is directly generalizable to the generation of continuously forced IGW trains, the relevance of our findings to continuously forced numerical simulations and the laboratory is also discussed. Finally, the question is posed whether, it is physically possible in the ocean or atmosphere, for a robust large-amplitude and vertically localized IGW packet to be generated and, moreover, propagate sufficiently far from its origin in the atmosphere or ocean while maintaining its original structure and amplitude.

2 Problem description and numerical method

We are primarily interested in examining the generation and propagation (and breaking, when desired) of a large-amplitude hydrostatic IGW packet such as that considered in previous investigations [22,31]. The horizontal wavelength of such a wave is much bigger than its vertical wavelength, and accordingly, it has near-horizontal group velocity. Note that the findings of this paper are also relevant to nonhydrostatic IGWs.

The governing equations are the two-dimensional, incompressible Navier–Stokes equations under the Boussinesq approximation:

$$\frac{\partial \mathbf{u}}{\partial t} = -\mathbf{u} \cdot \nabla \mathbf{u} - \frac{1}{\rho_0} \nabla p' + \nu \nabla^2 \mathbf{u} - g \frac{\rho'}{\rho_0} \hat{\mathbf{k}} + F_{\mathbf{u}}, \quad (1)$$

$$\frac{\partial \rho'}{\partial t} = -\nabla \cdot (\mathbf{u}(\rho' + \bar{\rho}(z))) + \kappa \nabla^2 \rho' + F_{\rho}, \quad (2)$$

$$\nabla \cdot \mathbf{u} = 0, \quad (3)$$

where $\mathbf{u} = (u, w)$ and the terms p' and ρ' represent the perturbations of pressure and density from their respective (mean) reference values which are in hydrostatic balance [7]. The wave packet is generated through the body force terms, $F_{\mathbf{u}} = (F_u, F_w)$ and F_{ρ} . The forcing terms are patterned after the initial condition often used in IGW process studies, a wave packet at time $t = 0$ as represented by a solution of the inviscid, nondiffusive linear internal wave equations [31]:

$$u_w(x, y, t = 0) = U_o \left(-\frac{Am}{k} F(z) \cos \phi - \frac{A}{k} F'(z) \sin \phi \right), \quad (4)$$

$$w_w(x, y, t = 0) = U_o A F(z) \cos \phi, \quad (5)$$

$$\rho_w(x, y, t = 0) = - \left| \frac{d\rho}{dz} \right| \frac{U_o A}{\omega} F(z) \sin \phi, \quad (6)$$

where $\phi = kx + mz$, m and k are the vertical and horizontal wave numbers, ω is the angular frequency, U_o is a reference velocity scale and A is the nondimensional amplitude of the vertical velocity, such that AU_o is the vertical velocity amplitude of the generated wave packet. Consistent with the definition used by Slinn and Riley in their study of continuously forced IGW trains [22], the forcing terms, $F_{\mathbf{u}}$ and F_{ρ} , result from dividing (4)–(6) with a reference time scale L/U_o (where the reference lengthscale is $L = \lambda_x = 2\pi/k$) and replacing the phase argument with $\phi = kx + mz - \omega t$. We use the same localization function used by Slinn and Riley [22] and Winters and D'Asaro [31]:

$$F(z) = \exp \left(-\frac{(z - z_{\text{cen}})^2}{2\sigma^2} \right), \quad (7)$$

which, however, we recast in terms of the half-height σ of the localization function. The particular choice of σ is such that the Gaussian envelope of this function fits about four vertical wavelengths.

The baseline case around which all simulations are designed is patterned after that considered by the critical level interaction study of Winters and D'Asaro [31]. The problem geometry is illustrated in Fig. 1. Two possible configurations are considered in a linear stratification: one where the generated IGW freely propagates away from the generation region and one where it encounters a Gaussian jet that is positioned several vertical wavelengths away from the wave source. The latter configuration is briefly discussed in §3.4 and presented elsewhere in greater detail [1].

There are four physical parameters that can be varied independently in the current numerical model; the strength of the stratification as measured by the Brunt Vaisala frequency (N); the kinematic viscosity of the fluid (ν); the wave's vertical velocity amplitude (AU_o); and the angle that the wave number forms with the horizontal direction ($\theta = \arctan(m/k)$). Now, in terms of identifying the relevant nondimensional parameters of the problem, we define a wave-based Reynolds number, $Re_w = C\lambda_x/\nu$ (where $C = \omega\lambda_x$ is an approximate horizontal phase speed), and Richardson number, $Ri_w = (N\lambda_x/C)^2$. As a consequence of the wave dispersion relation ($\omega = N \cos(\theta)$; see [26]), the two nondimensional parameters can be related to N , ν , θ through $Re_w = N \cos(\theta)\lambda_x^2/\nu$ and $Ri_w = (1/\cos(\theta))^2$. Accordingly, for complete specification of the physical parameters of the numerical model, one needs to specify the wave-based Reynolds and Richardson number along with the vertical velocity amplitude. Finally, it is to be noted that the wave number inclination angle $\theta \approx 83^\circ$ and hence $Ri_w = 65$ in all of the simulations reported in this study. Hence, the key numerical model parameters are Re_w , AU_o .

To enable a straightforward comparison with the work of Winters and D'Asaro [31], we also consider an alternative Richardson number denoted by $Ri = (N\lambda_x/U_o)^2$. This particular definition of Ri allows us to find the appropriate N (and hence Re_w) for a given U_o and λ_x to achieve dynamic similarity with the case considered by Winters and D'Asaro [31] (provided that viscous effects are minimal as in the simulations reported in

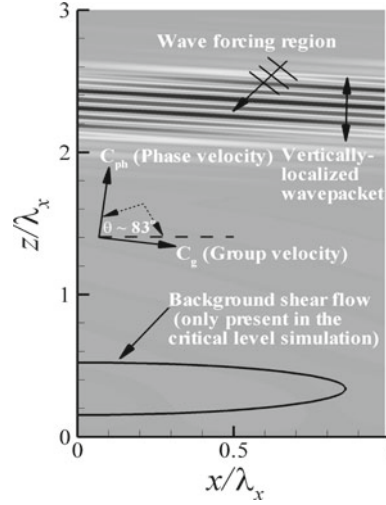


Fig. 1 Schematic of problem setup: a vertically localized IGW is generated in the forcing region and allowed to freely propagate downward. In the critical level simulation (see also reference [1], a Gaussian background shear flow is positioned near the bottom of the computational domain.

Table 1 Parameter values used in the base-case simulation

Parameter	Value
Ri	1
Ri_w	65
Re_w	1.5×10^6
Pr	1
m/k	8
A	0.015
L_x/λ_x	1
L_z/λ_x	3
σ	$L_x \sqrt{(0.21)^2 / (-2 \ln(1/2))}$
z_{cen}/L_z	0.8

Winters and D’Asaro [31]). Note that throughout this manuscript, ω and N are used in units of rad/s (including the definitions of Ri_w and Re_w). For the purpose of comparing with Winters and D’Asaro, the definition of Ri considers N in units of Hz. Table 1 summarizes the values of the parameters used in the baseline case for the free propagation simulations. It is emphasized that, for the baseline case, $Ri = 1$, $Re_w = 1.5 \times 10^6$, and $A = 0.015$. The value of A in the base case, which is the same as in the large amplitude case studied by Winters and D’Asaro [31], is such that the steepness of the wave field is $\simeq 96\%$ the overturning limit (defined as $\cot \theta / (2\pi)$ in reference [25]) for the particular angle θ . Finally, an additional set of simulations is considered where the stratification frequency N is increased by a factor of 4, leading to a value of $Ri = 16$ and $Re_w = 6 \times 10^6$.

The rectangular computational domain has dimensions L_x and L_z . In all simulations, L_x is chosen to accommodate one horizontal wavelength, with the exception of the runs investigating the effect of horizontal localization where L_x is adjusted accordingly (see §3.2). L_z is selected to allow for a domain where the generation region is sufficiently far from the top and bottom boundaries to avoid unwanted reflections and to allow sufficient distance for the wave to propagate downward through the ambient fluid. The boundary conditions are periodic in the horizontal direction and, at the top and bottom, free-slip for the velocity and no-flux for the density perturbation. In all simulations, the forcing is turned on and off impulsively (i.e., without any gradual ramp-up and ramp-down in amplitude) and is kept active for exactly one wave period, up to time $T_w = 2\pi/\omega$.

The resulting vertically localized wave packet, hereafter referred to as the “mature wave packet”, is expected to have the specified frequency and wave lengths and to propagate downward with the group velocity predicted by the linear theory.

Through a series of preliminary runs, the forcing amplitude input to the numerical model is iteratively adjusted so that by the end of the forcing period, the mature wave packet will have the nominal vertical velocity amplitude AU_0 .

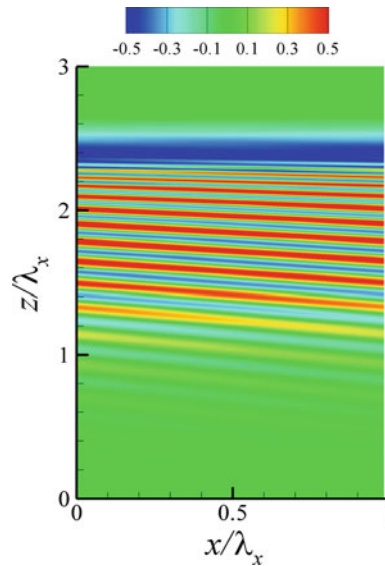


Fig. 2 Two-dimensional contours of the horizontal velocity field at $t = 5T_w$ in a fully nonlinear simulation of a horizontally periodic, vertically localized wave packet, for $Ri = 1$ (contours are normalized by the horizontal velocity amplitude $A_u = AU_{om}/k$ at $t = T_w$)

The numerical method used is a spectral multidomain penalty method model developed for the simulation of high Reynolds number incompressible Boussinesq flows in vertically finite domains [7]. Use of the penalty scheme in the vertical and explicit spectral filtering preserves the spectral accuracy and numerical stability at the scales of physical interest for high Reynolds number flows where simulations are commonly under-resolved. Fourier spectral discretization is employed in the horizontal, whereas in the vertical, a Legendre multidomain collocation scheme is used. The baseline grid resolution for the free propagation simulations consists of 64 grid points in the horizontal and 25 vertical subdomains of equal height and uniform order of polynomial approximation of 40, for a total of 1025 vertical grid points. Adaptive time stepping is used (based on 3rd order backward differentiation and stiffly stable schemes) with a maximum time step of $2\pi N^{-1}/60$.

3 Results

3.1 Horizontally periodic and vertically compact wave packet

We first examine results from fully nonlinear numerical simulations for the baseline case of a horizontally periodic and vertically compact IGW ($Ri = 1$ or equivalently $Re_w = 1.5 \times 10^6$). Two-dimensional contours at $t = 5T_w$ of the horizontal velocity field (Fig. 2) show a horizontally homogeneous band of negative flow created behind the rear of the wave packet. Focusing on one-dimensional vertical transects and as the generated wave packet moves downward, a progressive reduction in its amplitude is observed along with strong structural modulations and distortions of its rear flank (see Fig. 3). By $t = 5T_w$, the wave packet has decayed to nearly half its originally prescribed amplitude. Note that the asymmetry that develops in the wave envelope prevents a consistent/accurate definition of the wave amplitude at $t = 5T_w$.

Such a relatively weak and structurally modified wave packet may not be suitable for numerical simulations directed toward exploring the amplitude sensitivity of strong wave intensification and breaking. Presumably, the decay of the wave packet's amplitude can be compensated for by the use of larger initial forcing amplitude. However, since the wave amplitude considered here is very close the overturning limit at the given wave number orientation angle, the initial amplitude cannot be increased any further without risking the breaking of the wave at the source.

Figure 4 shows the evolution of the mean horizontal velocity profile, defined as

$$U(z, t) = \frac{1}{\lambda_x} \int_0^{\lambda_x} u'(x', z, t) dx', \quad (8)$$

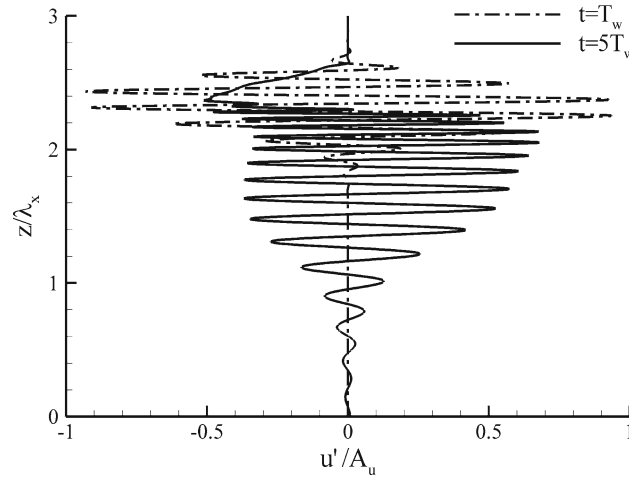


Fig. 3 Vertical profile of the instantaneous horizontal velocity at $x = L_x/2$ at $t = T_w$ and $5T_w$ in a fully nonlinear simulation of a horizontally periodic, vertically localized wave packet, for $Ri = 1$

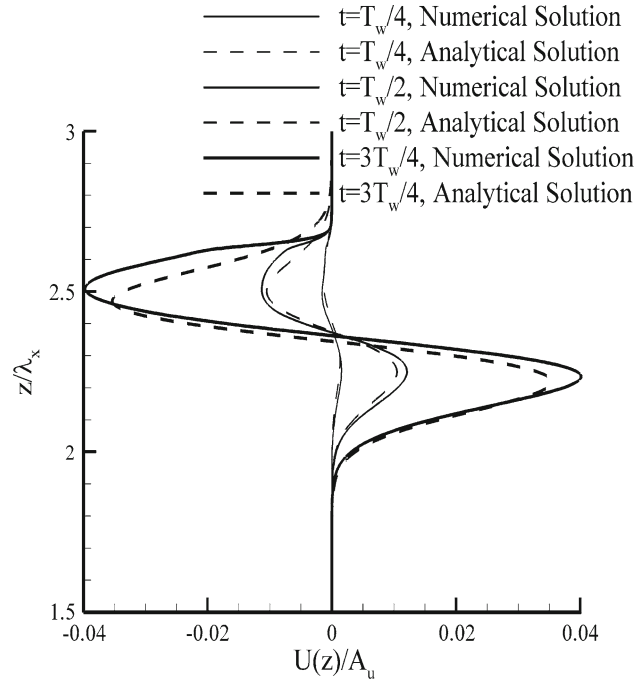


Fig. 4 Comparison of the analytical and numerical solutions of the mean flow evolution during the wave generation phase in a fully nonlinear simulation of a horizontally periodic, vertically localized wave packet, for $Ri = 1$

during the wave generation phase. As is visible in Fig. 4 and also in contour plots of the instantaneous horizontal velocity at much later times (not shown here), the mean flow is associated with two counter-flowing horizontal jets that develop in the forcing region. As shown in the subsequent discussion of §3.3.3, the negatively oriented jet remains localized in the forcing region as a residual mean flow. It is found to grow nonlinearly with time by, apparently, depleting the IGW packet of its energy and producing strong structural modulations. Finally, §3.3.3 also establishes that the positive component of the horizontal jet corresponds to what has been identified in previous studies as the mean flow induced by the propagating wave.

An additional simulation, similar to the one described above, has been run where all parameter values are kept the same, except for the Brunt Vaisala frequency, N , which is now quadrupled ($Ri = 16$ or $Re_w = 6 \times 10^6$). In this case, the highly nonlinear near-source interaction of the IGW with the residual mean flow produces

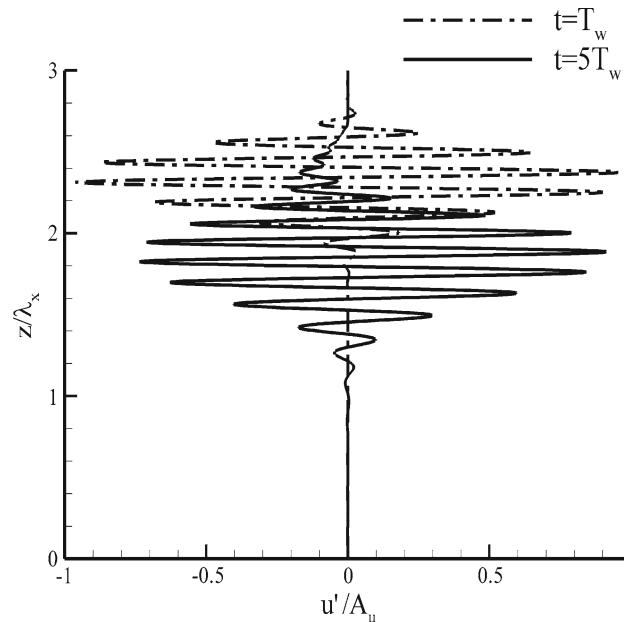


Fig. 5 Vertical profile of the instantaneous horizontal velocity at $x = L_x/2$ compared at $t = T_w$ and $5 T_w$ in a fully nonlinear simulation of a horizontally periodic, vertically localized wave packet, for $Ri = 16$

only a 20% decay of the wave's initial amplitude and significantly weaker structural modulations of the rear flank of the packet (Fig. 5).

3.2 Effect of horizontal localization

By virtue of the design of the forcing functions described in §2, the resulting IGW packets are infinitely periodic in the horizontal. In the laboratory and in nature, a more realistic wave source will have a finite extent not only in the vertical but also in the horizontal, thus generating waves that are localized in the horizontal. Such horizontal localization can have a significant impact on the evolution of large-amplitude IGWs [25]. Jones and Houghton [16] conjectured that a horizontally localized IGW source injects momentum into the mean flow in a horizontally limited region, thereby enabling the development of horizontal pressure gradients which, in turn, oppose the formation of mean currents.

A simulation has been performed in which the wave packet is compact in both the vertical and horizontal directions. The vertical localization function and governing parameters values are the same as those employed in the horizontally periodic case of §3.1. The combined/two-dimensional localization function is

$$F(x, z) = \exp - \left(\frac{(x - x_{\text{cen}})^2}{2\sigma_x^2} + \frac{(z - z_{\text{cen}})^2}{2\sigma_z^2} \right) \quad (9)$$

where, in order to avoid potential horizontal dispersion effects, σ_x is such that the horizontal envelope (defined as the interval spanning $\pm 10\%$ of the maximum value of 1 in $F(x, z)$) of the forcing encompasses two horizontal wavelengths. The horizontal domain dimension and resolution are quadrupled, with respect to those listed in §2, to prevent spurious interactions of the wave packet with its periodic image and to maintain the same number of horizontal grid points per wave length. The wave packet is initially centered at $x = L_x/2$, where the forcing itself remains centered throughout its entire duration (one wave period).

Two-dimensional contours of the horizontal velocity field (Fig. 6) at $t = 5 T_w$ show a significantly weaker, horizontally inhomogeneous, negatively oriented jet-like flow behind the rear of the wave packet. It can also be seen that the IGW packet has undergone weaker structural modulation at its rear end. A vertical profile of the instantaneous horizontal velocity sampled through the center of the wave packet at $t = T_w$ and $5 T_w$ (Fig. 7) shows that the wave packet at $t = 5 T_w$ has experienced only a 30% decay of its initial amplitude with much weaker structural modulations relative to its horizontally periodic counterpart. In § 3.3.4, we further explore

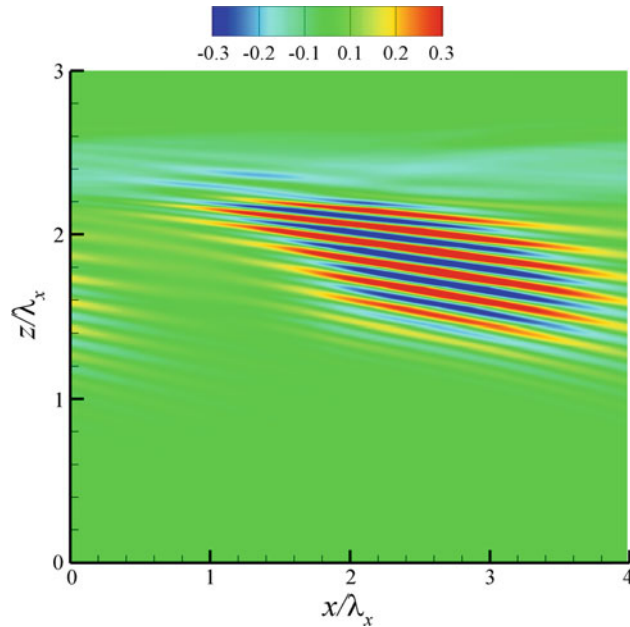


Fig. 6 Two-dimensional contours of the horizontal velocity field at $t = 5T_w$ in a fully nonlinear simulation of a both vertically and horizontally localized wave packet, for $Ri = 1$. Note the reduction in the *colorbar* limits as compared to Fig. 2, which is done to highlight the weaker mean flow and its horizontal inhomogeneity in the rear of the wave packet

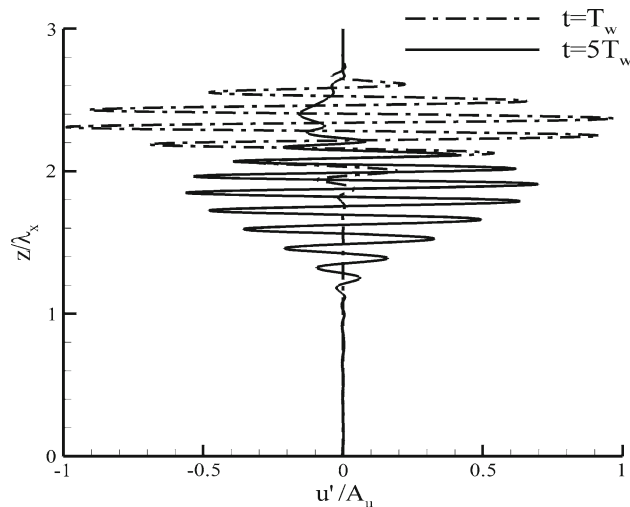


Fig. 7 Vertical profile of the instantaneous horizontal velocity at the instantaneous wave packet center, x_c , compared at $t = T_w$ and $5T_w$ in a fully nonlinear simulation of a both vertically and horizontally localized wave packet, for $Ri = 1$

the underlying cause for the observed reduction in the strength of the mean flow for the horizontally localized wave packet and assess the validity of the Jones and Houghton [16] conjecture on horizontal pressure gradients driving suppression of horizontal streaming of a horizontally localized IGW packet.

3.3 Model for wave packet deformation

3.3.1 Mean flow evolution equation and scaling

Decomposing the instantaneous velocity field $u(x, z, t)$ into the sum of a horizontal average (denoted by an overbar) $\bar{U}(z, t)$ and an associated perturbation $[u'(x, z, t), w'(x, z, t)]$, it can be shown that for

two-dimensional, nonrotating, stratified flow, which is statistically homogeneous in x (which is valid for an IGW that is infinitely periodic in the horizontal when the averaging interval is λ_x), the evolution equation for the mean horizontal velocity is given by

$$\frac{\partial \bar{U}}{\partial t} = -\frac{\partial \overline{u'w'}}{\partial z} + \nu \frac{\partial^2 \bar{U}}{\partial z^2}, \quad (10)$$

which is the same equation as that considered by Zikanov and Slinn [32] and Scinocca and Shepherd [21], with the latter focusing on the inviscid version. The mean flow is, therefore, driven by the Reynolds stress gradient and viscous attenuation. For ideal, space-filling IGWs, the Reynolds stress takes on a uniform value in the region occupied by the waves and thus cannot induce a mean flow. However, strong vertical localization can introduce non-negligible vertical variations in the Reynolds stress and, as a result, a strong mean flow. Lighthill [17] argued that in the laboratory, the mean force resulting from viscous attenuation can be canceled by horizontal pressure gradients that may be easily set up in a finite-size container (presumably due to free surface tilting).

By neglecting the viscous term (an assumption justified by the values of Reynolds number considered in this study), Eq. (10) simplifies to:

$$\frac{\partial \bar{U}}{\partial t} = -\frac{\partial \overline{u'w'}}{\partial z}. \quad (11)$$

Note that due to the periodicity of the forcing terms, they do not appear in both Eqs. (10) and (11). Thus, these equations represent the mean flow velocity that forms not only when the forcing is active but also when a localized IGW packet freely propagates away from the source region.

An estimate of the growth in the mean horizontal velocity of a vertically localized IGW packet during one wave period $T_w = 2\pi/\omega$ may be obtained by appropriately nondimensionalizing Eq. (11). The characteristic velocity and time scales are chosen to be $A_u = AU_o m/k = A_\zeta \omega \tan(\theta)$ and $1/\omega$, respectively. The characteristic length scale is that of the Reynolds stress variation in the vertical, i.e., σ . Equation (11) now becomes:

$$\frac{\partial U^*}{\partial t^*} = -\frac{A_\zeta \tan(\theta)}{\lambda_x \gamma} \frac{\partial \overline{u'^*w'^*}}{\partial z^*}, \quad (12)$$

where stars represent nondimensional quantities and $\gamma = \sigma/\lambda_x$. The growth of the mean horizontal flow over one wave period therefore scales with $A_\zeta \tan(\theta)/(\lambda_x \gamma)$, i.e., the mean flow is enhanced with increasing wave steepness and degree of vertical localization of the packet. Furthermore, mean flow formation is enhanced for wave packets that are closer to the hydrostatic limit ($\omega/N \ll 1$ for $\theta \rightarrow \pi/2$), i.e., near-horizontally propagating waves.

Alternatively, one can write

$$\frac{A_\zeta \tan(\theta)}{\lambda_x \gamma} = A/\sqrt{Ri} \frac{\tan(\theta)}{\gamma \omega/N}, \quad (13)$$

which quantifies the scaling of the mean flow velocity as a function of input parameters (see Table 1). Thus, Eq. (13) indicates that for a fixed nondimensional vertical velocity amplitude A , wave number inclination angle θ , and degree of vertical localization γ , wave packets operating in weaker stratifications are more susceptible to mean flow generation, as they are bound to have higher steepness (i.e., larger A_ζ/λ_x).

If one rescales the mean flow velocity profiles of the $Ri = 1$ and 16 cases with \sqrt{Ri} , the profiles are found to coincide at $t = T_w$, (Fig. 8). At $t = 5T_w$, the scaled profiles nearly coincide over their negative jet portion but show significant differences over the positive jet component. This deviation suggests that the proposed scaling does not accurately capture the highly nonlinear later stages of the wave-mean flow interaction (apparently intensified with the large wave steepness in the $Ri = 1$ case) in which the mean flow becomes strong enough to modify the initially prescribed wave field characteristics upon which the current scaling is based.

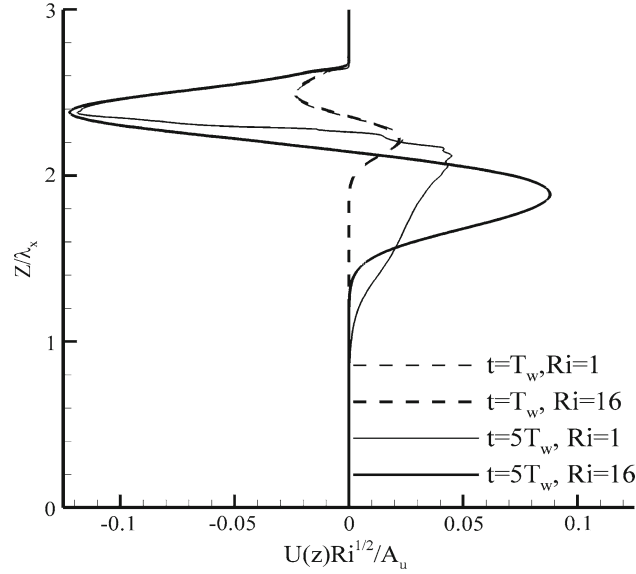


Fig. 8 Richardson number-rescaled mean flow profiles in fully nonlinear simulations of a horizontally periodic, vertically localized wave packet at $Ri = 1$ and 16

3.3.2 Approximate solution at early times

At sufficiently early time, i.e., when the forcing is active ($0 < t < T_w$), the mean flow is not found to grow enough to significantly alter the structure of the wave field. The early time evolution of the wave field may therefore be accurately predicted. As shown in §3.4, this prediction may be used in developing a mean flow containment technique. Specifically, it is reasonable to assume that the mature wave packet resulting from the application of the forcing to an initially quiescent flow field, has, to leading order, velocity and density fields that are given by Eqs. (4)–(6) with an amplitude $\tilde{A}(t)$ that grows in time and a time-dependent phase $\phi = kx + mz - \omega t$. Furthermore, assuming negligible dispersion, the wave envelope has a structure that is considered to remain unchanged in time and translates downward with the vertical component of the packet's group velocity, C_{gz} , as computed by linear theory. Our observations during the interval $0 < t < T_w$ confirm the above assumptions, which are invalidated as soon as significant mean flow begins to form, thus altering the originally prescribed spatial structure of the wave field.

The associated Reynolds stress distribution may now be written as

$$\overline{u'w'} = U_o^2 \left(-\frac{\tilde{A}^2(t)m}{k} \overline{\Phi^2(z, t) \cos^2 \phi} - \frac{\tilde{A}^2(t)}{k} \overline{\Phi(z, t) \Phi'(z, t) \cos \phi \sin \phi} \right), \quad (14)$$

where $\Phi(z, t)$ has the same structure as $F(z)$ in Eq. (7) but with z_{cen} replaced by $z_{\text{cen}} - |C_{gz}|t$ to account for the downward propagation of the wave packet. By evaluating the horizontal averages and substituting them back into (11), we have:

$$\frac{\partial \overline{U}}{\partial t} = U_o^2 \tilde{A}^2(t) \frac{m}{k} \overline{\Phi(z, t) \Phi'(z, t)}. \quad (15)$$

To proceed, the amplitude function $\tilde{A}(t)$ needs to be specified. In the simulations considered here, during the time of active forcing, the amplitude of the wave field is found to increase linearly with time as $\tilde{A}(t) = At/T_w$. An estimate of the initial mean growth may then be obtained by integrating Eq. (15) from $t = 0$ to some time $t < T_w$. For the purpose of integration, the wave packet is assumed fixed in space in a quasi-static sense; the time dependence of the argument of the Gaussian function, Φ , is not taken into account when carrying out the integration. This assumption is justifiable when the total integration time is comparable to T_w and, thus, small compared to the significantly longer wave packet's vertical propagation timescale λ_z/C_{gz} . The early-time mean flow is thus computed as

$$\bar{U}(z, t) = U_o^2 \frac{A^2}{T_w^2} t^3 \frac{m}{3k} \Phi(z, t) \Phi'(z, t) \quad t < T_w = \frac{2\pi}{\omega}. \quad (16)$$

The estimate for mean flow evolution predicted by Eq. (16) is compared to the mean flow obtained from the numerical solution of the fully nonlinear Navier–Stokes equations in Fig. 4 for the baseline case. The analytical estimate captures quite well the initial structure, amplitude, and growth rate of the numerically generated mean flow up to $t = 3/4T_w$, when the numerical results exhibit non-negligible, but still small, deviations from the analytical solution. Beyond this time and as the mean flow continues to grow, the wave packet undergoes significant distortions and is no longer faithfully represented by the velocity fields given by Eqs. (4)–(6). Consequently, the mean flow that is further generated can no longer be predicted by Eq. (16), as one must consider the changes in the wave velocity field structure. To this end, a fully nonlinear analysis is needed where the coupling between mean and wave velocity fields is bidirectional, unlike the unidirectional coupling from wave to mean flows described above. The use of forcing based on the solution of the linearized wave equations in a fully nonlinear system is thus further justified, as it only establishes the early time structure of the wave field before it gets significantly altered by nonlinear effects.

3.3.3 Mean flow structure at later times

It is instructive to compare the mean flow observed within the mature IGW packet, namely when it has moved sufficiently far from the source, with previous theoretical predictions. Specifically, the mean flow, derived for a conservative (unforced, inviscid) flow of a freely propagating low-amplitude IGW [21], may be closely approximated by the second-order-accurate expression for the pseudomomentum [25], namely:

$$M(z) = -\overline{\omega_y A_\zeta}, \quad (17)$$

where $\omega_y = \partial u' / \partial z - \partial w' / \partial x$ is the vorticity and $A_\zeta = \overline{\rho' / |d\rho/dz|}$ is the vertical displacement and the overbar denotes averaging over one horizontal wavelength (as in the previous two sections). Although the above expression is derived for small amplitude waves, Sutherland [24] showed, using fully nonlinear numerical simulations, that the above expression is still accurate within numerical truncation and round-off errors, even for wave amplitudes close to the breaking limit [27].

Figure 9a and b compare the computed wave pseudomomentum with the actual mean horizontal flow at $t = T_w$ and $5T_w$ for the $Ri = 1$ and $Ri = 16$ simulations, respectively. The initial structure of the mean flow, as discussed in §3.3.2, is composed of a positive and negative jet, whose structure is dictated by the term $\Phi(z, t)\Phi'(z, t)$ in Eq. (16). According to Fig. 9a and b, the wave pseudomomentum is not characterized by any negatively oriented flow, whereas its positive component strongly overpredicts the corresponding mean flow observed inside the source region.

As the forcing is turned off and the wave packet freely moves downward, the amplitude of the negative jet continues to grow at the expense of the decaying wave packet. By $t = 5T_w$, it becomes about half the horizontal velocity magnitude, A_u , for the $Ri = 1$ case. At the same time, in the $Ri = 16$ case, the negative jet amplitude is very close the vertical velocity magnitude $A_w = AU_0 = 1/8A_u$, which corresponds to a factor of $1/\sqrt{Ri} = 1/4$ reduction in the strength of the negative jet relative to the $Ri = 1$ case. Figures 3 and 5 show that during the same period, the wave packets have decayed by about 50 and 20% of their initial amplitude in the $Ri = 1, 16$ cases, respectively.

The growth of the negative jet has been further monitored in a special simulation where the height of the domain (and the vertical resolution) has been doubled. This growth is found to continue until the weakened and structurally modulated wave packet completely leaves the forcing region, leaving behind the negative jet as a steady-state residual mean flow (see Fig. 10). At this point, the mature wave packet propagates further out into the ambient and evolves independently of the generation mechanism and any interaction with the negative jet.

Now, the positive jet created during the forcing period remains attached to the wave packet and propagates with it away from the source. Since the concept of wave pseudomomentum does not apply to forced IGW packets, it is not unreasonable that it initially overpredicts the positive component of the mean flow. However, it does predict with increasingly better accuracy the mean flow associated with the mature wave packet once the wave packet has exited into the ambient fluid and is no longer subject to the influence of the negative jet. Accordingly, we refer to the positive jet as the “wave-induced” mean flow to differentiate it from the negative jet left behind in the source region, which is regarded as a “residual” mean flow.

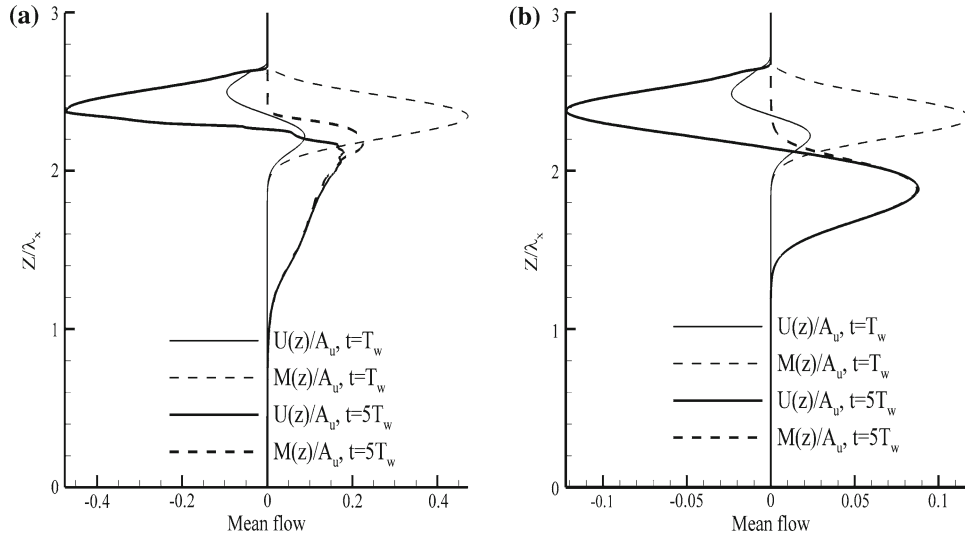


Fig. 9 Comparison of the mean horizontal flow profile and the wave pseudomomentum, $M(z)$, in a fully nonlinear simulation of a horizontally periodic, vertically compact wave packet at $t = T_w$ and $5 T_w$, for **a** $Ri = 1$ **b** $Ri = 16$

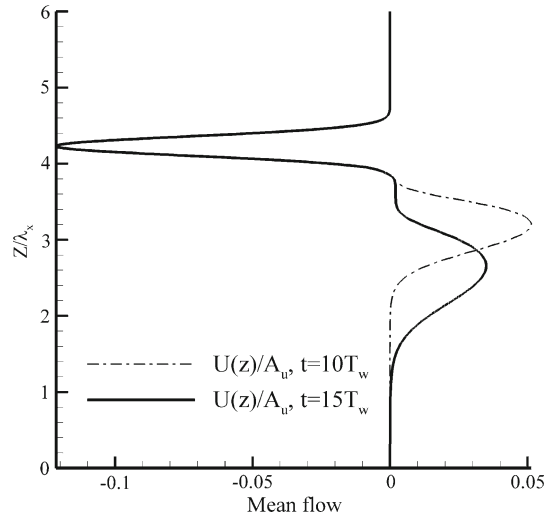


Fig. 10 Comparison of the mean horizontal flow profiles at $t = 10T_w$ and $15 T_w$, in a fully nonlinear simulation of a horizontally periodic, vertically compact wave packet in a domain with height $L_z = 6\lambda_x$, for $Ri = 16$

For the $Ri = 16$ run (Fig. 9), the near-Gaussian shape of the computed wave-induced mean flow is consistent with the shape of the mean flow reported in the low-amplitude simulations of Sutherland [25, 28]. At $Ri = 1$ and $t = 5T_w$ (Fig. 9), however, the wave-induced mean flow exhibits a nonsymmetric profile, with a more diffuse leading edge and a peak near the rear flank of the packet, agreeing qualitatively with the general shape of the mean flow in the more hydrostatic ($m/k = 2.5$) of the large amplitude cases examined by Sutherland [25], which is less hydrostatic than the wave considered here. The agreement of the wave-induced mean flow and the predicted pseudomomentum is worse at $Ri = 1$, i.e., the case with larger steepness, especially near the trailing edge of the packet, than for the $Ri = 16$ case. This is apparently caused by the stronger coupling between the wave and the mean flow in the $Ri = 1$ case.

3.3.4 Mean flow reduction due to horizontal localization

Understanding the cause underlying the observed reduction in the mean flow generated by a horizontally localized wave packet requires an appropriate definition of the horizontal averages of velocity and momentum

fluxes to enable objective comparisons with the corresponding metrics for a horizontally periodic wave. To this end, the horizontal mean of a variable $a(x, z, t)$ is defined as

$$\bar{a}(z, t) = \lim_{\ell \rightarrow \infty} \frac{1}{\ell} \int_{x_0}^{x_0+\ell} a(x, z, t) dx, \quad (18)$$

where ℓ is the sampling interval length. For the mean to be well defined, the limit must be independent of the initial location x_0 around which the limit is sought. While for a horizontally periodic IGW packet the averaging is clearly independent of the initial location x_0 , for a horizontally localized packet the limit is a function of where the averaging interval starts (i.e., x_0). For a horizontally limited IGW packet with a primary horizontal wavelength λ_x , it is possible to separate the wave form into an equivalent mean (as defined by Eq. 18) and a pure periodic wave-like component through phase averaging. Specifically, the phase average operator $\langle \cdot \rangle$ is defined as (see references [10,20])

$$\langle a(x, z, t) \rangle = \bar{a}(z, t) + \tilde{a}(x, z, t) = \lim_{N \rightarrow \infty} \frac{1}{N} \sum_{n=1}^N a(x \pm n\lambda_x, z, t). \quad (19)$$

The phase-averaged wave form $\langle a(x, z, t) \rangle$ is therefore the ensemble average of a sequence of all points along the x direction which have the same phase with respect to a reference wavelength (here taken as the IGW horizontal wavelength λ_x). Moreover, $\tilde{a}(x, z, t)$ is a horizontally periodic signal with a wavelength λ_x . However, on account of the horizontal variation of the ‘‘local’’ energy density per wavelength inside the horizontally localized IGW packet, the amplitude of $\langle a(x, z, t) \rangle$ is less than the maximum value of the original wave, $a(x, z, t)$. The desired horizontal mean $\bar{a}(z, t)$ can then be retrieved from the phase-averaged wave form by taking its horizontal average over one wavelength λ_x , i.e.,

$$\bar{a}(z, t) = \overline{\langle a(x, z, t) \rangle}, \quad (20)$$

since the average of $\tilde{a}(x, z, t)$ vanishes. The quantity $\overline{\langle a(x, z, t) \rangle}$ may then be directly compared to its counterpart for a horizontally periodic wave. Note that, computationally, the sum over N in Eq. (19) is limited to the effective width of the wave packet (defined as the interval spanning $\pm 10\%$ the maximum value of $u(x, t)$ at the particular z -location) to avoid artificial damping of the mean field $\langle a(x, z, t) \rangle$.

Now, consider the conservative form of the inviscid horizontal momentum equation for the wave field namely

$$\frac{\partial u'}{\partial t} = -\frac{\partial u'u'}{\partial x} - \frac{\partial u'w'}{\partial z} - \frac{\partial p'}{\partial x}. \quad (21)$$

Taking the phase average of both sides of Eq. (21) followed by the horizontal average, we obtain

$$\frac{\partial \bar{U}}{\partial t} = \underbrace{-\left\langle \frac{\partial u'u'}{\partial x} \right\rangle}_I - \underbrace{\left\langle \frac{\partial u'w'}{\partial z} \right\rangle}_{II} - \underbrace{\left\langle \frac{\partial p'}{\partial x} \right\rangle}_{III}, \quad (22)$$

where $\bar{U}(z, t)$ is the mean horizontal velocity. By numerically evaluating each of the three terms on the right-hand side of (22), one can identify the dominant term which drives the observed mean flow formation.

Figure 11 compares the vertical profiles of the sum of the r.h.s. terms of Eq. (22), $I + II + III$, normalized by (A_u/T_w) to the vertical profile of the second term $II/(A_u/T_w)$. We have found (not shown) that both the pressure gradient term III and the horizontal gradient of the wave Reynolds stress term I strongly oscillate in the vertical with a phase shift such that their individual profiles tend to cancel each other out. It can be seen from Fig. 11 that indeed the r.h.s. of Eq. (22) is dominated by the vertical gradient of the wave Reynolds stress. The sum of all three terms fluctuates around $II/(A_u/T_w)$ with a standard deviation of about 14%. The dominance of the second term in Eq. (22) is found to persist over the course of the entire simulation.

The magnitude of the vertical gradient (not shown) of the wave Reynolds stress at $t = T_w$ for the horizontally localized wave is found to be approximately half of the corresponding value for the horizontally periodic wave. This reduction in the strength of the Reynolds stress gradient is nearly commensurate with the observed reduction in the strength of the mean flow of the horizontally localized packet (computed by phase

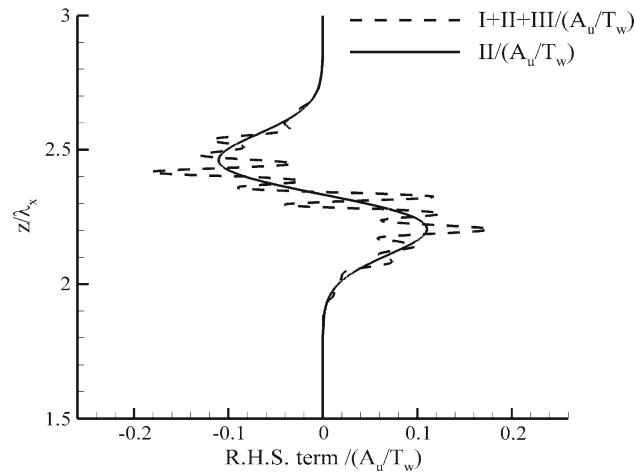


Fig. 11 Vertical profiles of the sum of all the r.h.s. terms of Eq. (18), $(I+II+III)/(A_u/T_w)$, and the second term $II/(A_u/T_w)$, in a fully nonlinear simulation of a horizontally as well as vertically localized wave packet at $t = T_w$, for $Ri = 1$

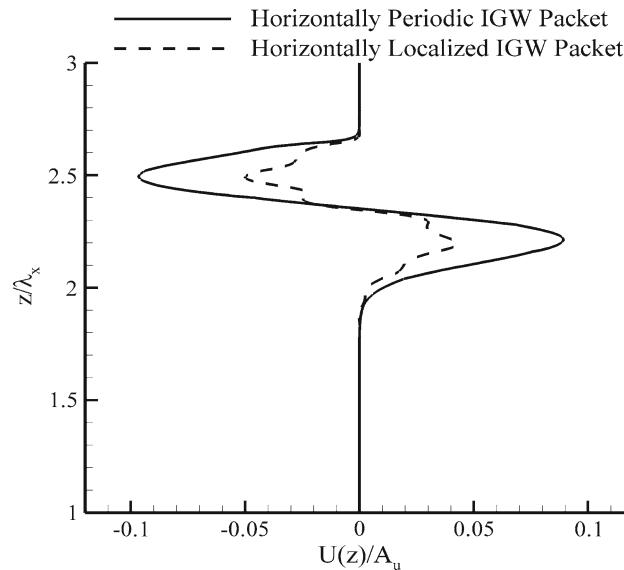


Fig. 12 Comparison of the numerical computed horizontal mean flow for a horizontally periodic and a horizontally localized IGW packet at $t = T_w$, for $Ri = 1$

averaging followed by horizontal averaging of the horizontal velocity field) with respect to the mean flow of the horizontally periodic packet (Fig. 12)

The mean flow reduction in a horizontally localized IGW packet, when compared to its horizontally periodic counterpart, is thus primarily driven by the reduced magnitude of the vertical gradient of the wave Reynolds stress which stems from the reduced wave energy density per horizontal wavelength. Both the horizontal gradient of the Reynolds stress and the horizontal pressure gradient play a secondary role in the evolution of the horizontal mean flow. Therefore, Jones and Houghton's [16] conjecture of horizontal pressure gradients reducing the mean horizontal flow is not valid.

3.4 Residual mean flow containment techniques

Two different strategies are considered toward containing the residual mean horizontal flow in the forcing region to prevent any disruptive interactions with the propagating wave packet. To this end, i.e., to enable the formation of a robust mature wave packet but also to prevent the spurious suppression of energy transfer to a

pre-existing mean flow (a background current in mid-water/air or along a boundary), the particular technique under consideration must be switched off at an appropriate time or be restricted to the wave generation region which, by design, should be sufficiently removed from the interaction region.

The first mean flow containment technique relies on assuming a horizontally periodic wave field. It involves the explicit removal of the mean horizontal flow component from the corresponding instantaneous velocity component after each time step. The approach is similar to that of Zikanov et al. [32], who, however, remove the plane average of the along-slope velocity component, as this direction is periodic, statistically homogeneous, and normal to the gravity vector (they note that any mean flow component in the up/down slope will be opposed by gravity and should be minimum). In the first phase of their simulation, they activate the mean flow removal technique throughout the computational domain. However, to avoid artificial suppression of the along-slope current in the second phase of their simulation, where the waves approach the sloping boundary and reflect off of it, the mean current removal is restricted to the upper 60% of the computational domain.

For the problem geometry considered here, i.e., a two-dimensional rectangular domain where the x-direction is normal to the gravity vector, the mean flow can be removed by setting to zero the zero Fourier mode of the horizontal velocity field. The zero Fourier mode deactivation region is delineated by a slowly varying window with a broad Gaussian envelope which smoothly couples the forcing region with the exterior fluid. This technique may be readily implemented in codes using Fourier discretization in the horizontal and is easily adaptable to algorithms using other discretizations (e.g., finite volume or finite difference) in horizontally periodic domains. In the latter case, one can directly calculate the mean flow through Eq. (8) and subtract it off the horizontal velocity field after each time step.

Motivated by Eq. (15), another technique for mean flow removal is now proposed. The technique involves the incorporation of a sink term in the r.h.s. of the horizontal momentum equation. The term is equal and opposite in magnitude to the rate of change of the mean horizontal flow. For the horizontally periodic wave packet, the form of this absorbing term is simply the negative of the r.h.s. of Eq. (15):

$$F_t = -U_o^2 \tilde{A}^2 \frac{m}{k} \Phi(z) \Phi'(z). \quad (23)$$

The $U_o^2 \tilde{A}^2 \frac{m}{k}$ factor in the above forcing term is approximated by the product of the absolute value of the instantaneous horizontal and vertical velocities at the center of the wave packet after each time step. The vertical coordinate of the instantaneous wave packet center is calculated as the location in the vertical profile of the wave packet's horizontal velocity (sampled at $x = L_x/2$) where an absolute maximum is attained. This location serves as the instantaneous origin for the functions $\Phi(z)$ and $\Phi'(z)$.

Two separate simulations have been run where each of the mean flow containment techniques is implemented throughout the full duration of the simulation for an IGW packet in the absence of any background flow. An additional run has been performed where the nonlinear terms are "turned off" but the zero Fourier mode is left untouched for the entire run. The results from all three cases are compared in Fig. 13. The mean flow is identically zero when either the nonlinear terms or the zero Fourier mode is absent. Thus, as indicated by Eq. (10), the observed wave-induced mean flow is driven by nonlinear effects with no energy deposited in higher horizontal harmonics. When a sink term is used, a very weak mean flow develops over the course of the simulation. When examining the wave packet's instantaneous structure in Fig. 14, it can be seen that, apart from dispersion effects typical of large-amplitude IGWs, the wave packet has preserved its initial spatial structure and decayed by less than 5% of its initial amplitude.

The first of the two above techniques has been successfully applied to the simulation of a critical level interaction of a horizontally periodic IGW packet (not shown here), with simulation parameters chosen to match the baseline case described in Table 1. The zero Fourier mode removal was restricted to the forcing region for the entire duration of the simulation. The background current was configured to be the same as that used in the simulation of Winters and D'Asaro [31]. Variable-thickness vertical subdomains were clustered around the initial location of the critical layer and its immediate neighborhood to ensure sufficient resolution of the wave-shear flow interaction. Upon arrival at the interaction region of the robust IGW packet, which preserved its originally prescribed features, an acceleration of the background shear flow was observed (which agrees with the results of Winters and D'Asaro. Furthermore, through a gradual quadrupling of the horizontal resolution enabled through a regridding procedure [18], localized Kelvin-Helmholtz instabilities developed all along the critical layer region in agreement with the observations of Winters and D'Asaro [31] and Lin et al. [18]. More details on the critical layer interaction simulation may be found in reference [1].

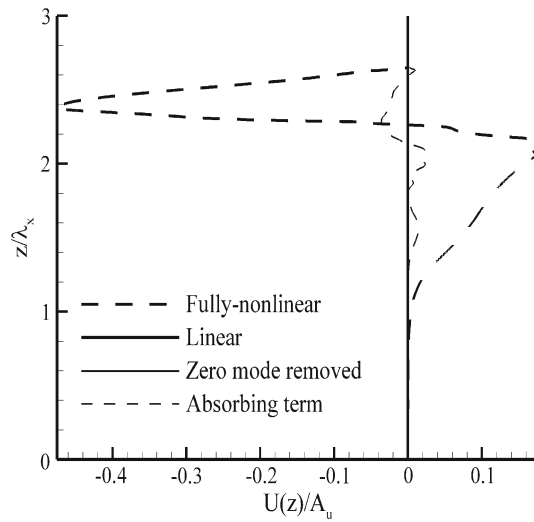


Fig. 13 Comparison of the mean horizontal flow in a fully nonlinear simulation and linear simulations, along with simulations in which either the zero Fourier mode is removed or the proposed mean flow absorbing term is used, for a horizontally periodic vertically localized wave packet at $t = 5T_w$, with $Ri = 1$ (note that the mean flow is zero everywhere in both the linear simulation and that with the zero Fourier mode removed)

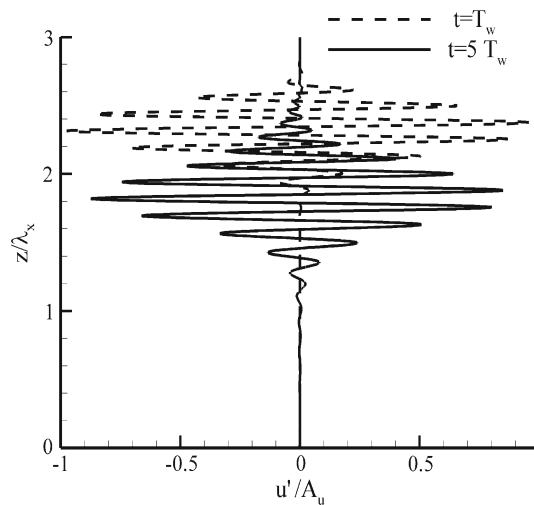


Fig. 14 Vertical profile of the instantaneous horizontal velocity at $x = L_x/2$, compared at $t = T_w$ and $5 T_w$ in a fully nonlinear simulation of a horizontally periodic vertically localized wave packet in which the mean flow absorbing term is used, for $Ri = 1$

4 Discussion

4.1 Mature wave packet: generation via mechanical forcing versus impulsive introduction

The focus of the present study is on the numerical generation of IGW's through the incorporation of explicit forcing terms into the governing equations. Forcing terms serve as a more generalizable approach which is amenable to the generation of either wave packets or continuous wave trains. However, the results of this work are also applicable to simulations of IGW's with equivalent initial conditions. In this case, when a mature wave packet is directly introduced, with the initial wave velocity and field prescribed by Eqs. (4)–(6), there is no mean flow present at time $t = 0$ by virtue of horizontal periodicity. Following the analysis of §3.3.2, the initially developing mean flow will establish the same spatial structure with the forced system. The early-time growth rate of the mean flow is linear and with a constant growth coefficient $\dot{A}(t) = A$. In contrast, in the forced system, the mature wave packet, which requires one wave period to form, is already accompanied by a weak mean flow (see Fig. 8) that has developed with a cubic growth rate as indicated by Eq. (16). For

both cases, the later stages of the wave- mean flow interactions are expected to be similar to what is described in §3.3.3. As the core of the interaction occurs once the forcing has been switched off after one wave period, the weak mean flow established after one wave period in the forced approach is not likely to significantly alter the wave residual mean flow interaction, compared to the equivalent interaction in the initial conditions approach.

However, through other mechanisms than those described above, the presence of forcing may enhance the accumulation of energy in the forcing region in the form of a nonpropagating component of the solution, as compared to an equivalent simulation with initial conditions. Specifically, it can further be argued that because the forcing is abruptly turned on and off, additional (typically higher) frequencies are introduced beyond the primary frequency. Also as the vertical Gaussian envelope of the forcing narrows in the physical space, its spectral support increases, resulting in the introduction of additional vertical length scales beyond the primary vertical wavelength of the wave packet. For a specified horizontal wavelength, these additional vertical length scales may not match either the forcing frequency or the additional frequencies introduced by the transient nature of the forcing, and the associated energy may remain trapped in the source region. Note, however, that several test simulations were run in which the forcing terms were gradually ramped up and down over an interval $[0, 2T_w]$. On one hand, little reduction in the strength of the residual mean flow component was observed. On the other, the resulting wave packet developed an envelope that was broader than originally prescribed.

4.2 Generation of an internal wave train

Issues with mean flow formation are also relevant in the framework of the continuous generation of IGWs, as already reported by Zikanov and Slinn [32]. What they describe as a “transient mean flow associated with the propagating front of the wave” is near equivalent to the mean flow induced by the mature wave packet. The mean flow generated in their forcing region, however, is the equivalent of the negative jet discussed in §3.3.2 and §3.3.3. In terms of the problem geometry they consider, the establishment of a statistically steady state of wave reflection (and possible breakdown into turbulence) near the bottom boundary requires persistent injection of energy into the vertically limited forcing region to generate a wave train. Over longer times, on account of the vertical gradient of the Reynolds stress that is established in the forcing region (see also Eq. 12), a non-negligible residual mean flow will inevitably develop therein which will significantly alter the propagating wave packet through the mechanism described in §3.3.2 and §3.3.3. Despite differences in the nature of the wave forcing (body force terms in the governing equations vs. physical wave generator; see the next section), such a mechanism may not only be operative in numerical simulations but also in equivalent laboratory experiments, as the formation of disruptive horizontal currents that significantly contaminate the source region has been reported to us (T. Peacock, personal communication).

4.3 Additional connections with the laboratory and nature

In a computational setting, the use of a body force term in the governing equations allows for the fluid within the source region to move freely. In contrast, in the laboratory, the internal wave generator is a mechanical device within which no fluid motion is possible [12]. Furthermore, lab-space limitations require that such a device be inevitably localized in the horizontal, which is expected to significantly reduce the mean flow, as suggested by §3.2. In addition, any externally imposed incidental horizontal pressure gradients may also act to oppose horizontal streaming, as proposed by Lighthill [17]. Most importantly though, confinement effects of the tank/container walls in a small-scale facility can strongly impede the formation and sustenance of a horizontal mean flow.

In the ocean and atmosphere, IGWs are usually generated by a source of finite scale and, as a result, have dimensions that are comparable to those of the source, as suggested in references [2, 13]. Furthermore, in such settings, horizontal and vertical confinement are typically not an issue. Thus, under sufficiently strong and vertically localized periodic forcing, strong residual horizontal currents could be produced for either IGW packets or wave trains at the respective generation site. A favorable situation where this may happen is a sufficiently nonlinear internal tide operating over a particular geometry of bottom topography in the deeper ocean [19].

5 Concluding remarks

The formation of strong mean horizontal flows has been examined in two-dimensional numerical simulations of internal gravity wave (IGW) packets where the waves are generated by incorporating mechanical forcing terms into the incompressible Navier–Stokes equations. The observed mean flows are, in part, a direct result of modeling the vertically localized forcing based on a solution to the linearized inviscid internal wave equations, yet introducing it at large amplitude into the fully nonlinear governing equations. As a result, a vertically localized gradient in the Reynolds stress field emerges within the source region giving rise to an opposing horizontal current which distorts the prescribed structure of the IGW packet and depletes it of its energy as the wave packet moves into the ambient fluid. At early times, a simple mathematical model, based on a unidirectional coupling from the wave to the mean flow, accurately predicts the spatial structure of the horizontal mean flow, which consists of two counter-flowing jets. The jet oriented against the horizontal group velocity of the wave packet remains trapped within the forcing region as a residual mean flow. The jet component aligned with the horizontal wave group velocity remains attached to the IGW as the wave propagates away from the forcing region. Sufficiently far from the source, the structure of the latter component of the mean flow is predicted reasonably well by the correlation of vertical displacement and vorticity fields.

Scaling arguments indicate that the mean flow is enhanced with a stronger degree of localization of the forcing, higher degree of hydrostaticity, and increasing wave packet steepness. Equivalently, it is enhanced with weaker stratification and higher IGW amplitude and degree of hydrostaticity. Horizontal localization is found to appreciably reduce the strength of the mean flow as a result of the reduced vertical gradient of the wave Reynolds stress field on account of the reduced wave energy density per wavelength.

In the particular flow solver under consideration, the mean flow may be eliminated by setting to zero the horizontal zero Fourier mode. A more generalizable approach consists of incorporating appropriately designed sink terms into the solver which also account for the propagation of the wave packet. With either of the above techniques, care must be taken that they are appropriately deactivated to avoid the spurious suppression of any physically driven mean flow formation as in the enhancement of flow along a sloping boundary or the transfer of momentum to a background current in mid-water or air.

The findings of this study are of particular value toward designing robust computational process studies of the above-mentioned types of remote interaction of an IGW packet (or a continuously forced wave train) where the wave amplitude range is required to be as broad as possible. Insight into the underlying physics of near-source horizontal currents in laboratory experiments of persistently forced IGW beams may also be obtained. Furthermore, we conjecture that similar horizontal currents may form in the flow of the oceanic internal tide over bottom topography in the strongly nonlinear regime.

An idealized numerical process study of the amplitude sensitivity of a remote interaction of a highly vertically localized and well-defined, in terms of envelope and primary frequency and wavelength, IGW packet, in which any distortions to wave structure and amplitude are contained through the approaches outlined in §3.4, is undoubtedly highly instructive. However, strong vertical localization is imposed by practical limitations in computational resources and not necessarily geophysical considerations. A process-focused simulation of a wave packet that is broader in the vertical can be prohibitively costly, especially when three-dimensional dynamics within the interaction region are of interest.

The concept of a “self-destructing” IGW was originally considered by Jones and Houghton [16]. Specifically, an initially weak-amplitude IGW packet, which has propagated upward, over sufficiently large distances, through a compressible atmosphere and a background density gradient decreasing with altitude, can experience significant amplification. This amplification may be of such an extent that the weak precursors of the wave at its leading edge are able to significantly modify the background flow state by creating a strong local mean flow in an otherwise quiescent atmosphere. As the bulk of the wave packet reaches the altitude where the mean flow has previously been created, a critical level forms and the wave breaks down and dissipates. While this common situation leads to strong modification of the wave structure and possible breakdown into turbulence, it happens far from the wave generation site (where the waves are presumably weak in amplitude during the wave generation) as large propagation distances are needed for significant wave growth.

The current study is focused on the near-source nonlinearities of an IGW packet (in an incompressible Boussinesq fluid) which can lead to intense structural changes within the generated wave field. A relevant though different inquiry may thus be posed: in nature, is it physically possible for a large-amplitude and strongly vertically localized IGW packet to form and, moreover, propagate over even a short distance away from its source (in what might effectively be a uniform stratification) while preserving a well-defined envelope and well-defined primary frequency and wavelength? Consequently, in a computational process study how

legitimate is it (in the context of the actual oceanic and atmospheric physics) to suppress any mean flow that develops within an IGW packet before any remote interactions occur? Both of these questions may ultimately have to be taken into account in the formulation of ray theory-based models [4] if and when large-amplitude IGW packets are considered.

Acknowledgments We are thankful to Professors B.R. Sutherland, D.N. Slinn, K.B. Winters and T. Peacock for illuminating discussions. We are indebted to Professor J.W. Rottman for providing valuable feedback on drafts of the manuscript and to Professor E.A. Cowen for guidance on phase averaging of localized wave fields. We thank two anonymous reviewers for a number of constructive comments. Support through Office of Naval Research grant N00014-08-1-0235 administered by Dr. Ron Joslin is gratefully acknowledged.

References

1. Abdilghanie, A.M.: A numerical investigation of turbulence-driven and forced generation of internal gravity waves in stratified mid-water. Ph.D. thesis, Cornell University (2010)
2. Appleby, J.C., Crighton, D.G.: Internal gravity waves generated by oscillations of a sphere. *J. Fluid Mech.* **183**, 439–450 (1987)
3. Boyd, J.P.: *Chebyshev and Fourier Spectral Methods*. Dover, Mineola (2001)
4. Broutman, D., Rottman, J.W., Eckert, S.D.: Ray methods for internal waves in the atmosphere and ocean. *Ann. Rev. Fluid Mech.* **36**, 233–253 (2004)
5. Campbell, L.J., Maslow, S.A.: Nonlinear critical-layer evolution of a forced gravity wave packet. *J. Fluid Mech.* **493**, 151–179 (2003)
6. Cushman-Roisin, B.: *Introduction to Geophysical Fluid Dynamics*. Prentice Hall, New Jersey (1994)
7. Diamessis, P.J., Domaradzki, J.A., Hesthaven, J.S.: A spectral multidomain penalty method model for the simulation of high Reynolds number localized stratified turbulence. *J. Comput. Phys.* **202**, 298–322 (2005)
8. Diamessis, P.J., Spedding, G.R., Domaradzki, J.A.: Similarity scaling and vorticity structure in high Reynolds number stably stratified turbulent wakes. *J. Fluid Mech.* (2010) (In Press)
9. Dohan, K., Sutherland, B.R.: Numerical and laboratory generation of internal waves from turbulence. *Dyn. Atmos. Oceans* **40**, 43–56 (2005)
10. Finnigan, J.J., Einaudi, F., Fua, D.: The interaction between an internal gravity wave and turbulence in the stably-stratified nocturnal boundary layer. *J. Atmos. Sci.* **41**, 2409–2436 (1984)
11. Fritts, D.C.: The transient critical-level interaction in a Boussinesq fluid. *J. Geophys. Res.* **87**, 7997–8016 (1982)
12. Gostiaux, L., Didelle, I., Mercier, S., Dauvois, T.: A novel internal waves generator. *Exp. Fluids* **58**, 123–130 (2007)
13. Hurley, D.G., Keady, G.: The generation of internal waves by vibrating elliptic cylinders. Part 2. Approximate viscous solution. *J. Fluid Mech.* **351**, 119–138 (1997)
14. Javam, A., Redekopp, L.G.: The transmission of spatially-compact internal wave packets through a critical level. *Dyn. Atmos. Oceans* **28**, 127–138 (1998)
15. Javam, A., Imberger, J., Armfield, S.W.: Numerical study of internal wave-caustic and internal wave-shear interactions in a stratified fluid. *J. Fluid Mech.* **415**, 89–116 (2000)
16. Jones, W.L., Houghton, D.D.: The self-destructing internal gravity wave. *J. Atmos. Sci.* **29**, 844–849 (1972)
17. Lighthill, J.: *Waves in Fluids*. University Press, Cambridge (1978)
18. Lin, C.L., Ferziger, J.K., Koseff, J.R., Monismith, S.G.: Simulation and stability of two-dimensional internal gravity waves in a stratified shear flow. *Dyn. Atmos. Oceans* **94**, 325–366 (1993)
19. Peacock, T., Echeverri, P., Balmforth, N.J.: An experimental investigation of internal tide generation by two-dimensional topography. *J. Phys. Oceanogr.* **38**(1), 235–242 (2008)
20. Reynolds, W.C., Hussain, A.K.M.F.: The mechanics of an organized wave in turbulent shear flow. Part 3. Theoretical models and comparisons with experiments. *J. Fluid Mech.* **54**, 263–288 (1972)
21. Scinocca, J.F., Shepherd, T.G.: Nonlinear wave-activity conservation laws and hamiltonian structure for the two-dimensional anelastic equations. *J. Atmos. Sci.* **49**, 5–28 (1992)
22. Slinn, D.N., Riley, J.J.: A model for the simulation of turbulent boundary layers in an incompressible stratified flow. *J. Comput. Phys.* **28**, 127–138 (1998)
23. Slinn, D.N., Riley, J.J.: Turbulent dynamics of a critically reflecting internal gravity wave. *Theor. Comput. Fluid Dyn.* **11**, 281–303 (1998)
24. Sutherland, B.R.: Internal gravity wave radiation into weakly stratified fluid. *Phys. Fluids* **8**, 430–441 (1996)
25. Sutherland, B.R.: Finite-amplitude internal wavepacket dispersion and breaking. *J. Fluid Mech.* **429**, 343–380 (2001)
26. Sutherland, B.R.: Internal wave propagation. In: Misra, J.C. *Modern Applied Mathematics*, pp. 372–422. Narosa Press, New Delhi (2005)
27. Sutherland, B.R.: Internal wave instability: wave-wave versus wave-induced mean flow interactions. *Phys. Fluids* **18**, 074,107 (2006)
28. Sutherland, B.R.: Weakly nonlinear internal gravity wavepackets. *J. Fluid Mech.* **569**, 249–258 (2006)
29. Thorpe, S.A.: On the reflection of internal wave groups from sloping topography. *J. Phys. Oceanogr.* **31**, 3121–3126 (2001)
30. Thorpe, S.A.: *The Turbulent Ocean*. Cambridge University Press, Cambridge (2005)
31. Winters, K.B., D’Asaro, E.A.: Two-dimensional instability of finite amplitude internal gravity wave packets near a critical level. *J. Geophys. Res.* **94**, 12,709–12,719 (1989)
32. Zikanov, O., Slinn, D.N.: Along-slope current generation by obliquely incident internal waves. *J. Fluid Mech.* **445**, 235–261 (2001)